Fuel 353 (2023) 129001

Contents lists available at ScienceDirect

Fuel

journal homepage: www.elsevier.com/locate/fuel

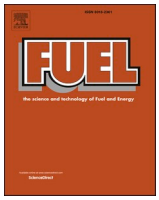

Full Length Article

Carbon-neutral and carbon-negative chemical looping processes using glycerol and methane as feedstock

Christopher de Leeuwe [a], Syed Zaheer Abbas [a], Alvaro Amieiro [b], Stephen Poulston [b], Vincenzo Spallina [a,*]

[a] Chemical Engineering, University of Manchester, Manchester M13 9PL, United Kingdom
[b] Johnson Matthey Technology Centre, Reading RG4 9NH, United Kingdom

ARTICLE INFO

Keywords:
Negative emissions
Glycerol reforming, hydrogen
Chemical looping

ABSTRACT

Carbon-negative and neutral methods to produce H_2 and other syngas-derived chemicals are tested and demonstrated in this study through chemical looping reforming of methane or glycerol. A chemical looping reactor provides the heat required to reform the glycerol or methane while having inherent CO_2 capture. This is achieved using dynamically operated packed beds. If the glycerol or methane is from a biological source this gives the system the potential for negative emissions. To evaluate the potential of this system, 500 g packed bed of oxygen carriers were cyclically reduced, oxidized, and used to carry out reforming experiments. The reforming process was tested at various pressure (1 – 9 bar) and temperature (600 – 900 °C). These conditions were tested at this scale for the first time. Complete conversion of glycerol is achievable with only small quantities of CH_4 slip. The maximum H_2 production was achieved at 1 bar and 700 °C producing a H_2/CO ratio of 10, this lowered to 9 when the temperature was increased to 900 °C. Adding CO_2 to the feed stream along with H_2O allows for a H_2/CO ratio suitable for the Fischer Tropsch (FT) synthesis. Chemical looping reforming of CH_4 with steam was successfully demonstrated in a lab reactor setup at 1 and 5 bar for multiple cycles with CH_4 conversion > 99% and controlled heat losses. The temperature and concentration profiles provided identical results for consecutive cycles verifying the continuity and the feasibility of the process.

1. Introduction

Hydrogen and gas-to-liquid (GTL) processes for ammonia, methanol and other gas-to-liquid processes are of vital importance in the global chemical products market. 60% of the global demand for these products is satisfied by the reforming of natural gas, oil and naphtha [1]. Alternative solutions to mitigate the environmental impact of the reforming process use bio-based sources in combination with carbon capture and storage (also called BECCS to result in negative CO_2 emissions [2,3].

Biogas is produced by the anaerobic degradation of organic matter by microorganisms [4]. The exact composition of biogas is highly dependent on the make-up of the feed. However, it predominantly consists of CH_4 (45–55%) and CO_2 (40–45%). The remainder is made up of N_2, O_2, and NH_3. There has been recent interest in increasing the production of biogas as it is produced from biological sources so any carbon captured during its generation, conditioning or utilisation would lead to negative emissions.

Crude glycerol ($C_3H_8O_3$) is the main by-product from biodiesel production by transesterification; 0.1 m^3 of it is produced for every 1 m^3 of biodiesel [5]. As the biodiesel industry continues to grow, its projected annual growth of 4.5% [5] will generate a surplus of glycerol for application. This large growth in biodiesel production has led to a surplus of glycerol.

The crude glycerol produced is contaminated with a high water content along with free fatty acids, salts, catalysts and other organic molecules giving it a dark brown colour. Crude glycerol requires a sequence of physiochemical treatments to salt content < 6% and for deep purification, the adoption of vacuum distillation or electrochemical processes is needed. [6]. When crude glycerol is originated from waste animal fats and in the case of 2nd generation bio-diesel plant, glycerol is categorised so that it cannot be sold as a product (regardless of the purity). Therefore it can be transformed into energy carriers such as H_2 or syngas for GTL technologies [7] removing the problem of hydrocarbons separation (separation (also known as matter

* Corresponding author.
E-mail address: vincenzo.spallina@manchester.ac.uk (V. Spallina).

https://doi.org/10.1016/j.fuel.2023.129001
Received 21 February 2023; Received in revised form 31 May 2023; Accepted 11 June 2023
Available online 11 July 2023

organics non glycerol, MONG) and water removal which is also needed for the reforming reactions. When combined with bioenergy carbon capture and storage (BECCS) this gives the ability to be a net negative contributor to atmospheric greenhouse gas concentrators or becoming carbon negative[2].

Compared to CH_4 reforming, $C_3H_8O_3$ reforming has more complex chemistry with, glycerol decomposition, water gas shift (WGS) and methanation reactions all occurring inside the reactor. However, crude glycerol's status as a waste stream from biodiesel production overcomes this shortcoming. This is highlighted by Equation (1)-Equation (5).

$$C_3H_8O_3 \leftrightarrow 4H_2 + 3CO\ \Delta H^o_{C_3H_8O_3} = 246.4\frac{kJ}{mol_{C_3H_8O_3}} \quad (1)$$

$$C_3H_8O_3 + 3H_2O \leftrightarrow 7H_2 + 3CO_2\ \Delta H^o_{C_3H_8O_3} = 122.8\frac{kJ}{mol_{C_3H_8O_3}} \quad (2)$$

$$CO + H_2O \leftrightarrow CO_2 + H_2\ \Delta H^o_{CO} = -41.2\frac{kJ}{mol_{CO}} \quad (3)$$

$$CH_4 + H_2O \leftrightarrow CO + 3H_2\ \Delta H^o_{CH_4} = 206.1\frac{kJ}{mol_{CH_4}} \quad (4)$$

$$CH_4 + 2H_2O \leftrightarrow CO_2 + 4H_2\ \Delta H^o_{CH_4} = 165\frac{kJ}{mol_{CH_4}} \quad (5)$$

There are various methods for glycerol reforming including steam reforming [8,9], dry reforming[10], partial oxidation[11], autothermal reforming [12], aqueous phase reforming [13,14], pyrolysis[15], and through microbial bio conversion[16].

These conventional reforming techniques for both Biogas and glycerol come at high operational and capital costs [17] and are dominated by two methods for reforming hydrocarbons in industrial strategies, namely steam and dry reforming in fired tubular reforming (FTR) and auto thermal reforming (ATR) [18]. Thermodynamic studies showed, for ATR, the optimal conditions for hydrogen production were temperatures between 625 °C and 725 °C [19], a glycerol-to-water ratio between 1:9 and 1:12, and an oxygen mole fraction of between 0 and 0.4 [20]. These result in high costs per ton of CO_2 avoidance (the avoidance cost of CO_2 is between 47 and 70 €/t depending on the capture rate and technology used) [18,21]. An alternative approach to produce syngas from glycerol would be to make use of chemical looping processes [22–24]. Chemical looping has been demonstrated to be an effective process to provide heating and achieve inherent CO_2 separation with near zero CO_2 emissions [22,25–29].

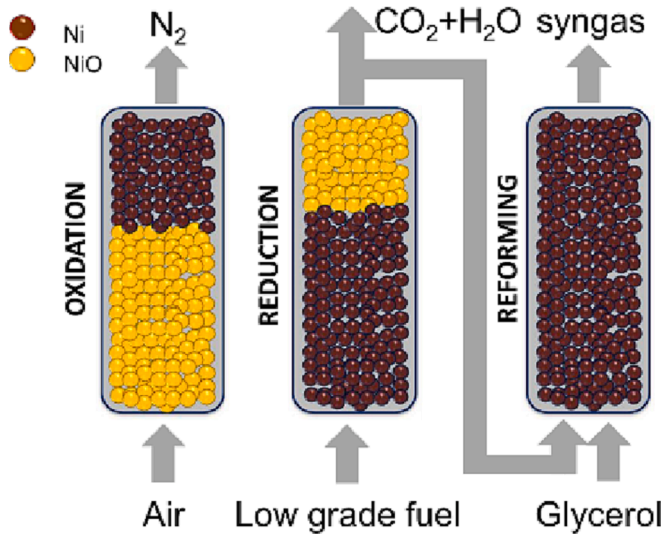

Fig. 1. Schematic of chemical looping reforming.

The separation is achieved through the use of a solid metal oxide also called oxygen carrier (OC) [30–33]. Literature work has focused on chemical looping fluidised bed systems [21–24] which work at atmospheric pressure. However, high pressure is preferable for industrial processes for both CO_2 removal and uses of syngas in downstream processes (methanol, ammonia, liquid fuel synthesis) so packed bed reactors have been proposed as an alternative [23,34]. Chemical looping reforming of CH_4 using CO_2 in packed beds has been shown to be capable of heat-neutral behaviour [27,29,35,36] with very promising economics for blue hydrogen production at small and large scales [27,37]. This study concentrates on the use of a chemical looping process for the conversion of glycerol to syngas which is represented in Fig. 1.

$$Ni + 0.5O_2 \rightarrow NiO\ \Delta H^o_{O_2} = -479.4\frac{kJ}{mol_{O_2}} \quad (6)$$

$$CO + NiO \rightarrow CO_2 + Ni\ \Delta H^o_{CO} = -43.26\frac{kJ}{mol_{CO}} \quad (7)$$

$$H_2 + NiO \rightarrow H_2O + Ni\ \Delta H^o_{H_2} = -2.125\frac{kJ}{mol_{H_2}} \quad (8)$$

First is the oxidation stage where the oxygen carrier (OC) reacts with air through Equation (6). This step is exothermic and it heats the solid inside the reactor. In the second stage, the feed gas is switched to one with a reducing potential by feeding waste gas (rich in CO, CO2, H2, and unreacted CH4) from a downstream process, for example uncondensable tail gases from Fischer-Tropsch (FT) reactor, and the OC is reduced through the Equation (7) and Equation (8). In the third stage, the glycerol reacts with H_2O and CO_2 to form syngas through the reaction Equations (1)–(5) (overall endothermic). The oxidation and then reduction of 1 mol of Ni using H_2 would produce 477.3 kJ of heat while reduction using CO would produce 436 kJ based on Equations (6)–(8) which, based on Equation (2) and (4) is sufficient to drive the reforming of 3.9–3.6 mol of glycerol or 2.3–2.1 mol of CH_4 producing more than enough H_2 or CO to complete the reduction. There is a sufficient margin that by controlling the ratio of the flowrates during the oxidation, reduction and reforming stages it is possible to achieve heat neutral behaviour even with the heat losses associated with a working plant.

This system can produce H_2 or CO using only air, water and either bio-methane or glycerol as feedstocks with separate waste streams of CO_2 mixed with H_2O, which can be easily separated by condensing H_2O, and N_2, which can be safely vented to atmosphere. This means that the system has a net negative carbon balance, reducing the CO_2 concentration in the atmosphere. Due to the high temperature achieved by the system (>800 °C), the CH_4 or glycerol are almost completely converted while the H_2/CO ratio is adjusted by using a proper H_2O/CO_2 ratio. Chemical looping reforming has previously been proven experimentally for Ni and Fe-based oxygen carriers at TRL 4 operating at 1–10 bar [35,36]. Further work has been carried out simulating dry reforming of CH_4 in chemical looping reactors highlighting the effectiveness of chemical looping reforming [38].Ni-based materials are mostly used as the reforming catalyst and OC due to the relatively low Ni precursor costs compared to expensive Pt group metals and its high glycerol steam reforming activity if using an Al_2O_3 support [39].

Glycerol-to-syngas conversion requires 123 kJ/mol of glycerol as the heat of reaction (Equation (2), most commonly approximately 190 kJ/mol of glycerol at temperature > 800 °C where glycerol is fully converted and a large amount of CO is present in the syngas (combination of Equation (1) and reverse Equation (3). As for other hydrocarbon reforming (e.g. natural, gas, biogas), the energy is provided by external fuel combustion leads to energy consumption and CO_2 emissions to the atmosphere (in the range of 0.15–0.3 $mol_{CO_2}/mol_{C_3H_8O_3}$). In case of chemical looping reforming, it has been already demonstrated that CO_2 is generated at high purity (thus available for utilisation or storage)

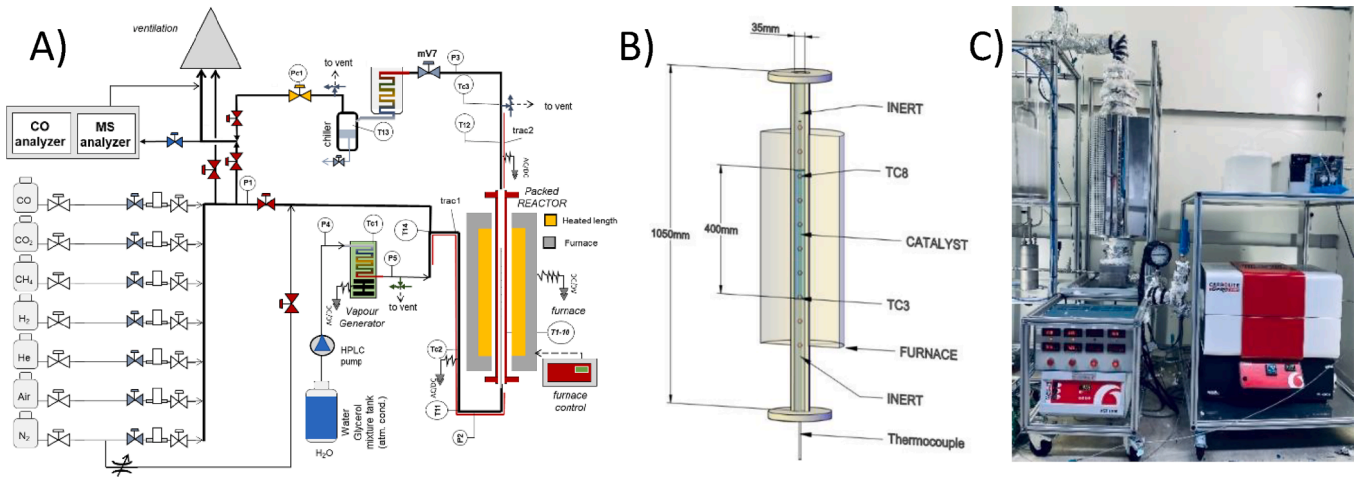

Fig. 2. Simplified schematic of the packed bed reactor system (A), cross section of the cross section of the packed bed reactor unit (B) and pictures of packed bed reactor system (C).

therefore the technology is more environmentally friendly and cheaper than other reforming technologies integrated with CO_2 capture ([28,29,33–37]). The same advantages also apply to the case of glycerol.

The vast majority of chemical looping glycerol reforming research has concentrated on the design of the OC without studying the effect of scale up[40–43]. However, some preliminary work at higher TRLs has been carried out albeit using fluidised bed systems at atmospheric pressure [44] or consists of purely theoretical studies of large scale plants for economics and thermodynamics[45–47]. This work aims to show that such a packed bed chemical looping reforming system would also be capable of carrying out steam or combined reforming of $C_3H_8O_3$ or CH_4. This will explore the optimum conditions and limitations of the steam methane reforming and glycerol reforming using 500 g of combined catalyst and oxygen carrier. Methane chemical looping reforming was tested at 1–9 bar, 600 to 900 °C and steam to carbon ratios of 2.5–4, while $C_3H_8O_3$ reforming was tested at 1 bar, 600 to 900 °C, a glycerol to water ratio of 12:1 and with the addition of CO_2 to achieve a 1:1 ratio of CO_2:H_2O. Full cycles of steam methane reforming will then be demonstrated for the first time at both 1 and 5 bar using a furnace at 600 °C to counteract the high degree of heat loss present at laboratory scale.

2. Methodology

A simplified schematic of the packed bed reactor setup used in this study is shown in Fig. 2. The setup consists of a high temperature resistant stainless-steel tube (253MA) with an inner diameter of 35 mm and length of 1050 mm (manufactured by Array Industries BV), a 6.3 mm ID multiple point thermocouple, with 10 measurement points, is used to obtain the unsteady axial temperature profile. Two different ten-point thermocouples were utilized; one with measurements every 75 mm which was used for glycerol reforming experiments and one with measurements every 50 mm which was used in the steam methane reforming. The reactor is heated using a jacketed furnace from Carbolite. To mitigate the heat losses, pipework before and after the reactor were insulated using ceramic wool. Gas feed flowrates are controlled by Bronkhorst mass flow controllers and pressure is controlled by a back-pressure regulator sensor (Bronkhorst). The reactor exhausts are cooled in an ice bath to remove any water content and the dry gas composition is measured using a combination of a mass spectrometer (Hiden QGA) and a CO analyser (Siemens).

There is additionally an HPLC pump (LC-20AP Shimadzu) for supplying liquid feeds to the system, these are fed to the system via a coiled pipe inside a separate temperature-controlled Carbolite furnace. A thermocouple at the end of the coil records the fluid temperature to ensure that all liquids have been vaporised. Heated lines are used outside the furnaces to maintain the pipework at 200 °C and to ensure no vapour condensation prior the reactor inlet.

Next to test the capabilities for chemical looping steam and mixed glycerol reforming, the middle of the reactor was packed with 440 g of 1st generation oxygen carrier based on Ni-supported on calcium aluminate manufactured by Johnson Matthey which has been tested in the past for the chemical looping reforming proof-of-concept [34,48] and recently demonstrated for high-pressure dry reforming [29,35]. This material was supplied in the form of a pellet of 12 mm size and crushed to a particle size of 1–1.4 mm (Fig. 3 A). Crushing was required to ensure a proper solid distribution inside the reactor and avoid gas channelling as the D/dp is < 30 [49]]. The total length of the reactive material inside the bed was 400 mm. This packed bed covered the thermocouples TC1-4 to TC1-8, with thermocouple TC1-3 located just before the start of the reactive section.

A second experimental campaign considered a new oxygen carrier formulation using 440 g of Ni on Al_2O_3 (Fig. 3 B), manufactured by Johnson Matthey. In this case, the material has been used as it. The total length of the reactor is 400 mm. The packed bed was fitted with a different multipoint thermocouple e with 50 mm spacing. The reactive section covered TC2.2 to TC2.8 with TC2-2 at the start of the reactive section of the bed.

3. Results and discussion

3.1. Glycerol reforming

The glycerol reforming catalytic activity of the material was first tested under the operating conditions matching those expected for industrial reforming applications. A 6 NLPM (normal litres per minute) of He and 64 g/hour (equivalent to 1.1 NLPM once vaporised) of a glycerol steam mixture with a molar steam to glycerol ratio of 12:1 (30% Glycerol by mass) was fed to the reactor. This was carried out between 700 and 900 °C at 1.0 bara. After steam reforming conditions had been tested, CO_2 was added to the feed to replace 1 NLPM of He at each temperature to assess the impact of combined dry and steam reforming reactions on the final syngas composition.

Both Fig. 4 and Fig. 5 show that steady reforming is achievable. The outlet gas composition and temperature at various points in the reactor do not change with a function of time. The carbon measured leaving the reactor was 0.22 ± 0.02 NLPM compared to the 0.25 NLPM in the feed, well within 2 standard deviations of the measurement. It can also be noted that there was no drop in temperature during the reforming stage maintaining the same temperature distribution across the bed throughout. The temperature is consistent during the reforming as the

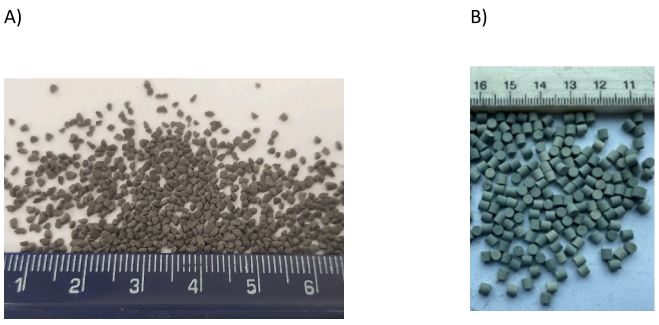

Fig. 3. A) 1–1.4 mm Ni-based OC supported on calcium aluminate and B) a 3 mm Ni-based OC on Al_2O_3 manufactured by Johnson Matthey.

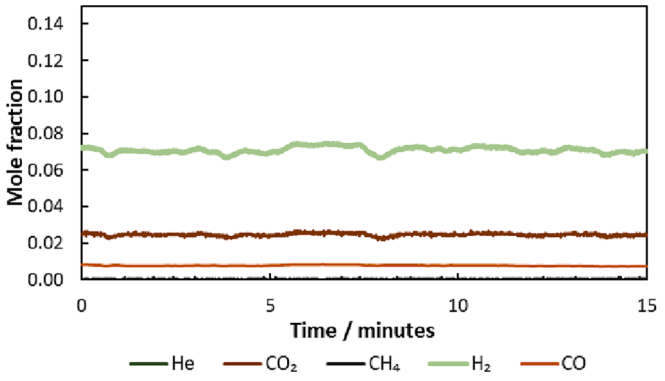

Fig. 4. Outlet gas composition profile during the glycerol reforming at 900 °C, 1 bar with a feed of 6NLPM He and 1 ml/min of liquid (12:1 water to glycerol ratio).

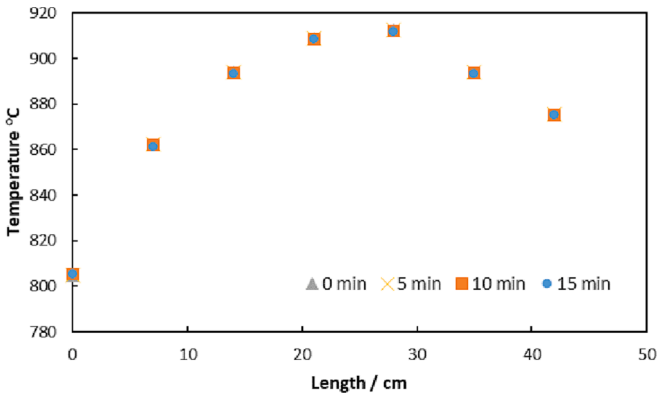

Fig. 5. Dynamic temperature profile during reforming at 900 °C, 1 bara, 6 NLPM He and 1 ml/min of liquid 12:1 water to glycerol at 0, 5, 10, and 15 min into the reforming.

heat required to drive the reforming experiment is supplied by the furnace. It can be seen that the temperature is lowest (803 °C) at the inlet of the reactor ($0 < z < 7$ cm), where most of the reforming occurs before increasing to a maximum value (910 °C) after 28 cm before dropping as the reactor reaches the end of the furnace where axial heat losses are very high. The temperature in the reactor exceeds the furnace set point at the near the middle of the reactor, this is caused by a combination of the furnace wall temperature being highest just above the midpoint of the reactor and the exothermic water gas shift reaction occurring after the glycerol is reformed. The exothermic reaction slightly heats the bed from the 900 °C set point to the 910 °C measured.

In case of steam reforming, the H_2:CO is equal to 9.0 which is suitable

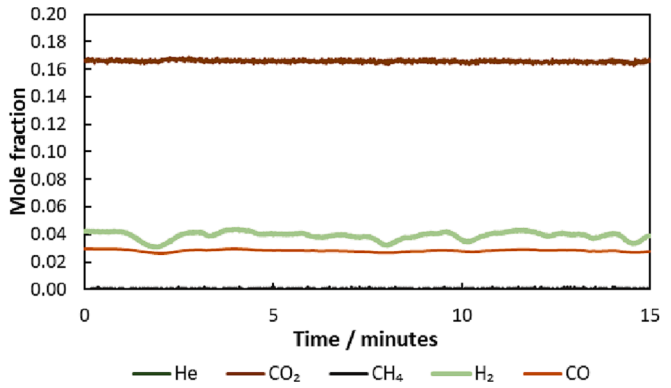

Fig. 6. Outlet gas composition profile during the glycerol reforming at 900 °C, 1 bar with a feed of 6NLPM He and 1 ml/min of liquid (12:1 water to glycerol ratio).

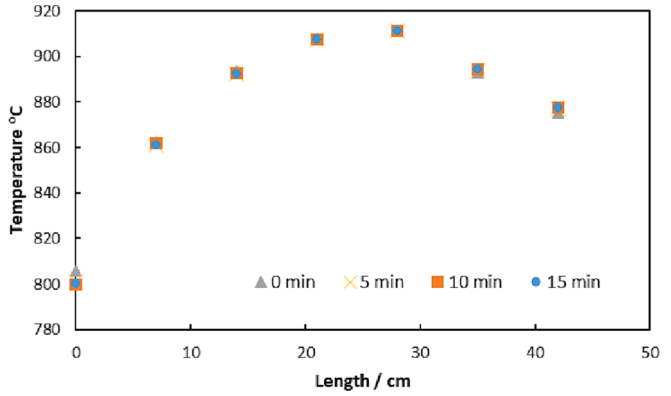

Fig. 7. Dynamic temperature profile during reforming at 900 °C, 1 bara, 6 NLPM He and 1 ml/min of liquid 12:1 water to glycerol at 0, 5, 10, and 15 min into the reforming.

for H_2 generation. In order to obtain a H_2:CO should be 1.8–2.0 for GTL application, CO_2 is added to the reactor to enhance both dry reforming and reverse water gas shift (RWGS) thus reducing the H_2 content while increasing CO. The same experiments were repeated with 5 NLPM of He and 1 NLPM of CO_2. The outlet gas composition and temperature profile can be seen in Fig. 6 and Fig. 7 respectively. A similar temperature profile along the bed is seen when comparing Figs. 5 and 7 with the reactor temperature exceeding the furnace set point due to the water gas shift reaction and this point having lower heat losses due to furnace wall temperature reaching a maximum at that point.

The amount of carbon leaving the reactor was 1.29 ± 0.04 NLPM compared to the 1.23 NLPM in the feed which is acceptable (a confidence interval of > 95%) It can also be noted that there was no drop in temperature during the reforming stage maintaining the same temperature at each point across the bed throughout the reforming. This is due to the furnace heating overcoming the endothermic nature of the $C_3H_8O_3$ reforming as well as any heat losses.

The outlet gas composition and H_2 to CO ratio (H_2:CO) from the experimental data were compared to the values predicted by a Gibbs reactor operated at the same setpoint of the furnace. This comparison is required to assess the deviation of the syngas composition with respect to experimentally measured ones as an indication of a suitable activity of the catalyst versus the reforming reaction. It can be seen in Fig. 8 that the system operates close to the thermodynamic limits suggested by a Gibbs reactor operated at the same setpoint of the furnace. Under steam reforming conditions the largest difference between the thermodynamic limitations and the experimental values was the CO mole fraction at 900 °C which was less that 1 mol% lower than the expected value with the

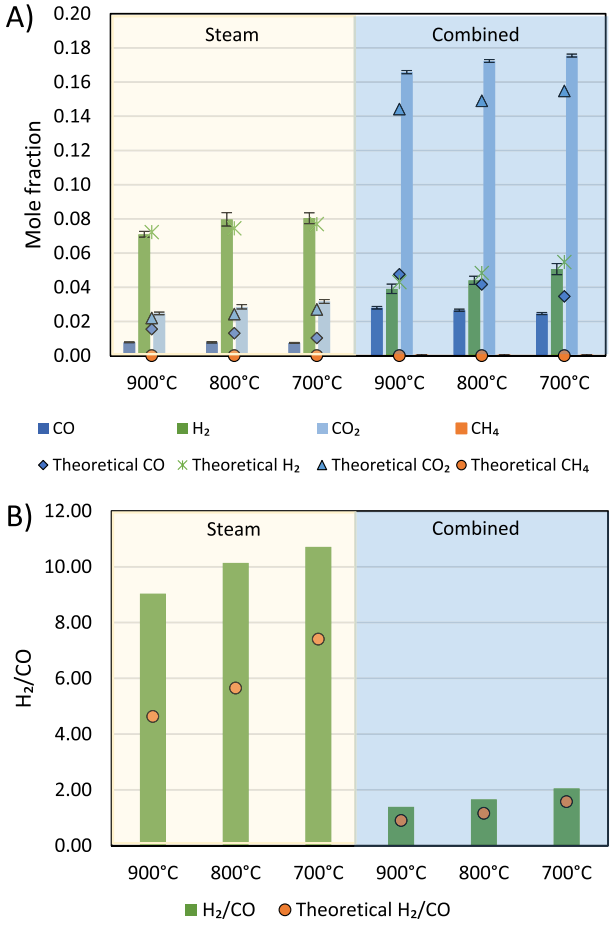

Fig. 8. A) Outlet gas composition during wet and combined reforming (steam + dry) at 1 bar 700–900 °C and B) H_2:CO ratio during wet and mixed reforming at 1 bar 700–900 °C, the high uncertainty is because the mole fraction of CO at the outlet is low at high temperatures, which in turn causes a large error to propagate through to the ratio calculation.

rest of the CO measurements similarly underpredicting the values. The difference in the CO value is most likely due to a combination of the colder temperature at the top of the reactor driving more WGS increasing the H_2 and lowering the CO and the higher CH_4 mole fraction that predicted lowering both the CO and H_2 mole fraction. This lower than expected CO mole fraction then causes the larger difference seen in the H_2/CO ratio as large percentage changes in the denominator causes large fluctuations in the value. This effect is also seen in the combined reforming results with increased CO_2 and decreased CO (maximum 2 mol% for CO and CO_2 at 900 °C) however these are a much lower percentage difference due to the increase in all carbon containing compounds due to the addition of the CO_2 to the feed.

Temperature profiles and outlet gas compositions as a function of time for these experiments can be found in Figures S1-S4 of the supplementary information. The material is a suitable catalyst for glycerol reforming and achieves results close to the thermodynamic limitations of such a system while the temperature is kept at 700 °C.

In our experimental setup, the direct glycerol measurement is not possible, however, the carbon balances for each case closes to within 2 standard deviations and the condensate collected during reforming had a density of 1000 kg/m^3 (pure water), and these both heavily imply complete conversion of glycerol. A small amount of CH_4 was produced during reforming (0.02 ± 0.05 mol%), which is consistent with literature findings for this material which has shown high CH_4 conversion when tested as a CH_4 reforming catalyst [35]. The H_2/CO ratio for each condition was higher than the ratio predicted by the Gibbs reactor, this is due to the lower temperature at the top of the reactor and throughout the remaining pipework, due to the fast kinetics for water gas shift reactions and low temperatures increasing H_2 and lowering CO content, it is expected that the outlet ratio would be higher than predicted by an isothermal reactor.

The GSHV values for the steam reforming was 1110 h^{-1} while for the combined reforming this increased to 1260 h^{-1}.

3.2. *Post glycerol reforming, oxidations, and reductions*

To confirm the suitability of the material for chemical looping reforming after the reforming, oxidations (at 600 °C, 1 bar, 10.5 mol% O_2 and 10 NLPM total flowrate) and reduction (at 900 °C, 1 bar, 20 mol % H_2 and 10 NLPM total flowrate) were carried out. The oxidation showed that no carbon deposition had occurred during the reforming with no CO or CO_2 seen in the outlet gas composition (Fig. 9). Furthermore, the material is shown to have good stability with the oxidations and reductions having the same oxygen transfer capacity (OTC). OTC was measured as 0.68 ± 0.02 mol of oxygen during oxidation and 0.66 ± 0.03 mol of oxygen during the reduction. This confirms the work carried out using the same material previously for dry methane reforming [35].

3.3. *CH_4 reforming stage*

In recent works [35,38], the authors have demonstrated the chemical looping dry reforming up to 5 bar using Ni on calcium aluminate. In this work, chemical looping reforming has been demonstrated up to the limit

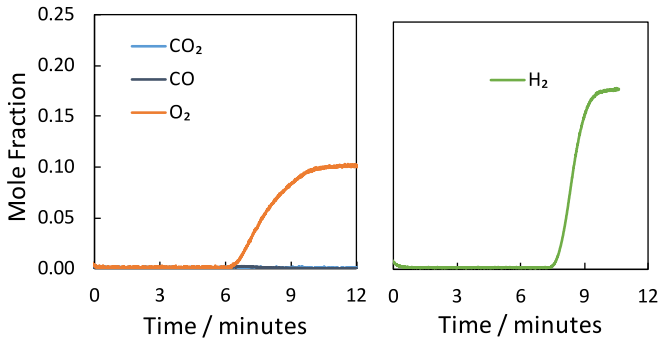

Fig. 9. Outlet gas composition during oxidation at 600 °C, 1 bar, 10.5 mol% O_2 and 10 NLPM total flowrate (A) using and reduction (B) at 900 °C, 1 bar, 20 mol % H_2 and 10 NLPM total flowrate.

Table 1
Experimental operating conditions during the steam reforming.

H_2O/CH_4	2.5:1	3:1	4:1
Flowrate (NLPM)	10	10	10
Initial bed temperature (°C)	600–900	700 – 900	700 – 900
Pressure (bar)	1 – 9	1 – 9	1 – 9
Gas composition (vol. %)			
He	10	10	10
N_2	55	50	40
H_2O	25	30	40
CH_4	10	10	10

of 9 bar using steam as an additional reactant under severe conditions to establish the boundaries and validate the process for the H_2 generation. The operating conditions used for the steam reforming are listed in Table 1.

The temperature profile and outlet gas composition during steam CH_4 reforming at 5 bar and 700 °C are shown in Fig. 10. While the start of the bed reduces in temperature rapidly, the rest of the bed maintains its temperature due to external heating. This trend is also explained by the fact that most of the CH_4 reforming occurs at the beginning in presence of Ni-based catalyst and high temperature. The gas composition at the outlet is steady after 5 min which is due to the time required to vent off the N_2 from the line downstream the reactor.

3.4. Effect of Temperature, pressure and Steam-to-Carbon ratio

Comparing different pressures, temperatures and gas compositions, steam reforming showed that the conversion of CH_4 behaved in line with thermodynamic predictions, with increased pressure limiting conversion, while higher temperatures and steam-to-carbon ratios increased conversion (Fig. 11). A temperature increase from 600 to 900 °C (5 bar and 3:1 S/C ratio) increased CH_4 conversion from 56.8% to 99.95% compared with the 60.7% to 99.8% predicted by the Gibbs simulation. Changing the S/C ratio from 2.5 to 4 (at 700 °C and 5 bar) increased CH_4 conversion from 83.7% to 92.1% compared with the 85.9% to 92.6% predicted by the Gibbs simulation. The Gibbs reactor over consistently over predicts the conversion in the reactor, this is due to a combination of kinetic limitations and the reactor not being isothermal with a cooler temperature at the top of the reactor. However the results closely follow each other at higher temperatures and low pressures and still provide insight at higher pressures and lower temperatures as the results still follow the same trends.

Similar patterns can be seen in the outlet gas composition, highlighted using the H_2:CO ratio in Fig. 12 with the predicted ratios lining up with the measured values, a slight deflection is seen at 600 °C for the 1 bar case which has a much larger ratio than predicted, this is due to a slightly lower conversion (80–90% depending on H_2O:CH_4 ratio) than predicted (85–95%) combined with the fractional nature of the ratio. However, the relationship to pressure remains the same with increasing temperature or decreasing H_2O:CH_4 increasing the H_2 content.

Throughout these experiments, the carbon balance closed to within 2 standard deviations and subsequent oxidation showed no CO or CO_2 highlighting the lack of carbon deposition during the reforming.

3.5. Complete chemical looping steam reforming cycle

A complete chemical looping CH_4 steam reforming sequence (CL-SMR) of operation has been performed for the first time in an experimental packed bed reactor at TRL-4 scale with repeated cycles and controlled heat losses at high pressure (Fig. 13). Compared to the previous work from the authors on dry reforming [35], in this work, sequences of 6 cycles at 1 bar and 5 cycles at 5 bar were performed continuously for 6 h. Oxidation, reduction and reforming inlet conditions have been tabulated in Table 2. The setpoint temperature of the furnace is kept at 600 °C during the entire time to reduce the heat losses of an experimental lab system. This temperature is chosen because the Ni-based OC presents good oxidation performance with T > 600 °C [35]. However, due to limitations of the liquid flow system the H_2O feed cannot be rapidly turned on and off so remains on throughout the cycle. This implies that H_2O is always present acting as an additional inert dilutant during oxidation and reduction. This technical challenge in feeding the reactor with liquid also makes full cycles of chemical looping glycerol reforming not possible as the $C_3H_8O_3$ would be present during the reduction and oxidation which does not make sense.

The complete cycles have been performed at 1 bar and 5 bar operating pressure. Initially, air (mixed with 10% He) was fed to the bed with the main products being N_2 and He as shown in Fig. 13. The oxidation continued until the O_2 breakthrough. After that, 4 NLPM of N_2 are used to purge the bed and remove any remaining O_2 in the reactor before the start of the reduction stage. During reduction with H_2, only H_2O is produced and N_2 is used as an inert carrier gas. A H_2O:CH_4 equal to 3 is used for the reforming stage. Catalytic reactions (SMR and WGS) take place in the part of the bed that is still in reduced form. The timings differ between the 1 bar and 5 bar experiments due to different purging requirements (dictated by gas velocity at different pressure) [35,36].

The outlet gases contain 28% H_2, 5% CO_2 and 4% CO under 1 bar pressure conditions and changes to 23% H_2, 2.6% CO and 5% CO_2 AT 5 bar. This change in gas composition can explained through the slightly different temperature profile at different pressures and the higher pressure lowering the CH_4 conversion from 99% to 97%. This shows that low pressure (1 bar) favours H_2 production as expected from the thermodynamics of the system. Fig. 14 shows the temperature profile during the one complete cycle of CLR at 1 bar and 5 bar operating pressures. Both cycles are consistent with the temperature at the beginning and end of each cycle matching. Both oxidations increase the temperature of the bed to similar temperatures. However, the longer purges and reduction required for the 5 bar case results in additional heat removal and therefore slightly lower temperature during the reduction and reforming.

The continuous testing campaign at 1 bar and 5 bar are shown in Fig. 15(A – B). After 600 s of reforming, the system is purged with 4 NLPM of N_2 to completely remove any fuel remaining in the bed and proceed to the next oxidation stage for the following cycle. 4 complete cycles represent good repeatability even though this system does not use an automated valve operation.

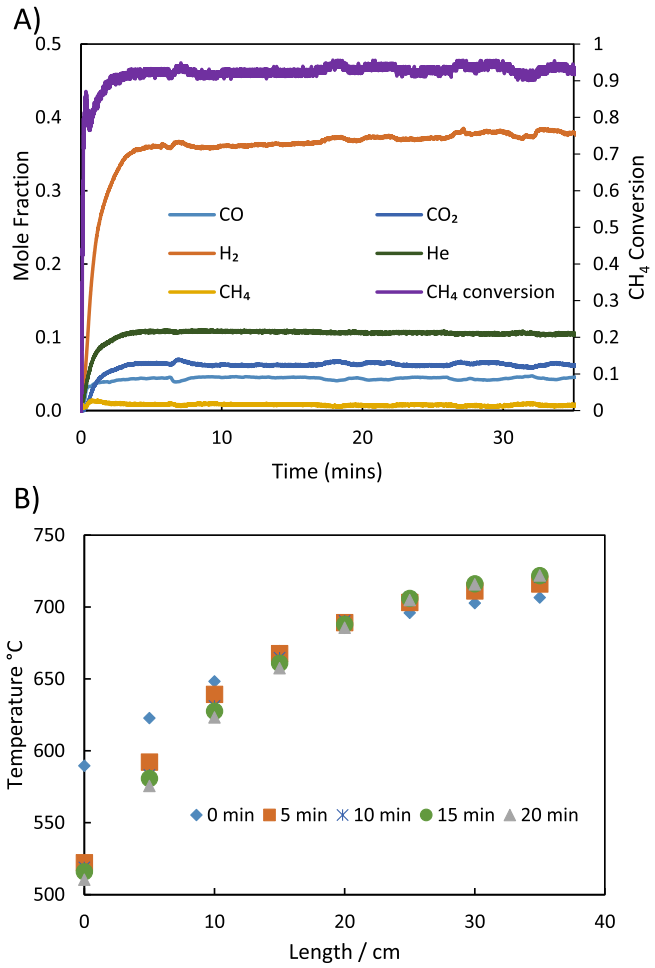

Fig. 10. Recorded temperature at 0, 5, 10, 15 and 20 min into the reforming (A), outlet gas composition and CH_4 conversion (B) during reforming at 5 bar, 10 NLPM feed flowrate, 700 °C initial bed temperature and 10% CH_4 and 40% H_2O in the feed.

3.6. Material characterisation

After undergoing testing samples of both Ni-based materials were analysed using SEM to determine any changes in morphology or degradation of the material. The 1–1.4 mm Ni on calcium aluminate material derived from crushing the tablet catalyst did not show any cracks or breaks in the particles tested Fig.16. The surface of the material is rough showing the beginnings of degradation.

In comparison, the Ni on Al_2O_3 with its larger particle size does seem to show the beginnings of cracks and pock marks on the surface

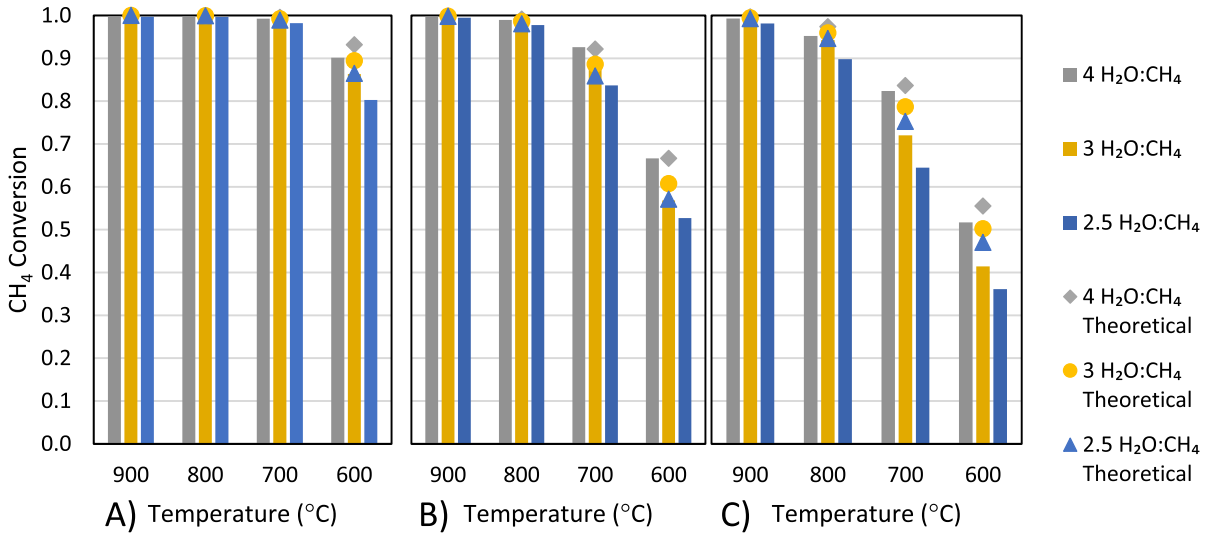

Fig. 11. CH_4 conversion as a function of temperature and S/C ratio compared with theoretical conversions for 1 bar (A), 5 bar (B) and 9 bar (C).

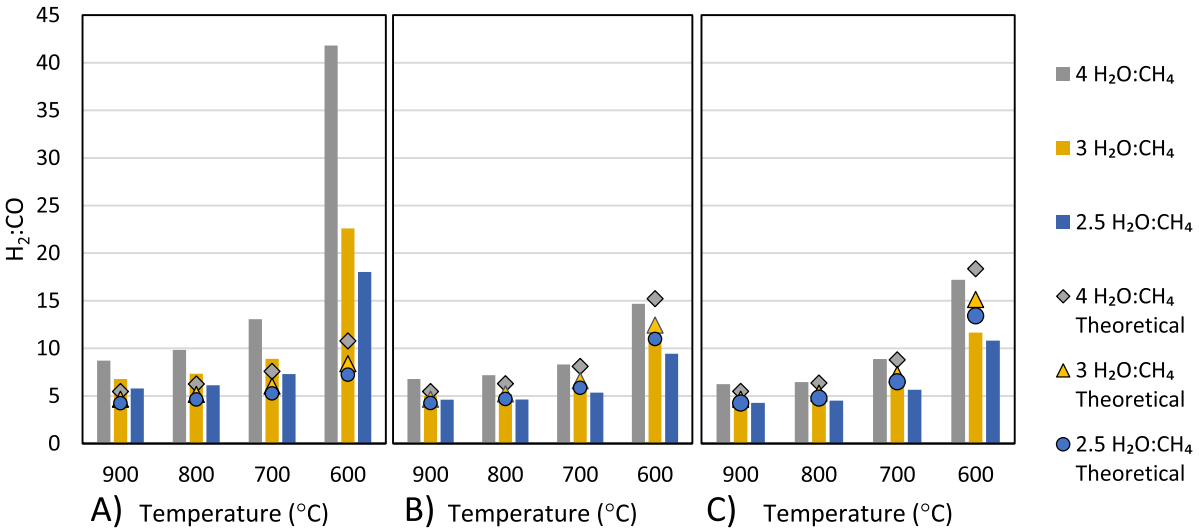

Fig. 12. H_2:CO ratio as a function of temperature and steam to carbon ratio compared with theoretical conversions for 1 bar (A), 5 bar (B) and 9 bar (C).

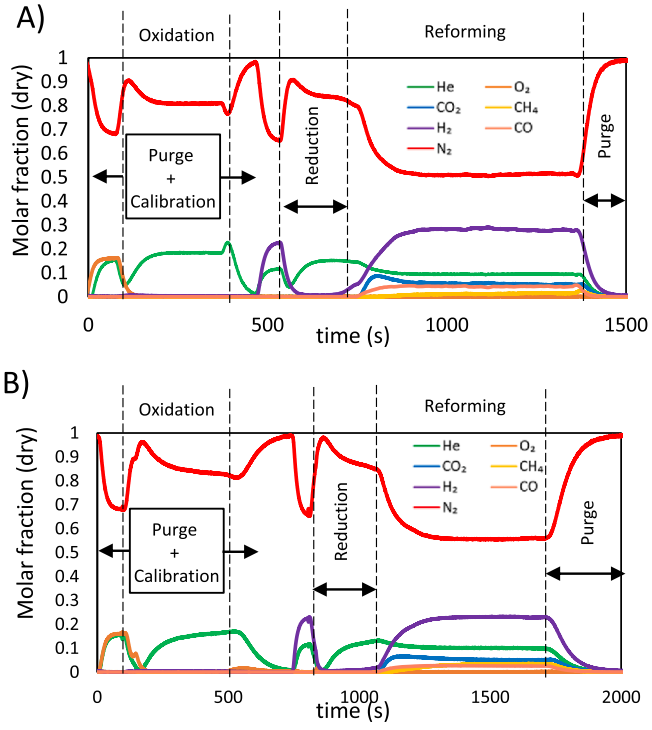

Fig. 13. Outlet molar fractions (dry) during the complete CLR cycle at A) 1 bar and B) 5 bar.

Table 2
Inlet operating conditions for the CLR complete cycle (furnace temperature at 600 °C and pressure at 1 bar and 5 bar).

Inlet conditions	Oxidation	Purge-I	Reduction	Reforming	Purge-II
FlowRate (NLPM)	10	5	14	14	13
Feed time (s)					
1 bar	300	200	200	680	280
5 bar	330	340	280	720	460
NLPM in FEED					
N_2	3.95	5	5	5	5
O_2	1.05	–			–
He	1	–	1	1	–
CH_4	–	–	–	1	–
H_2	–		2	–	
H_2O	3	3	3	3	3

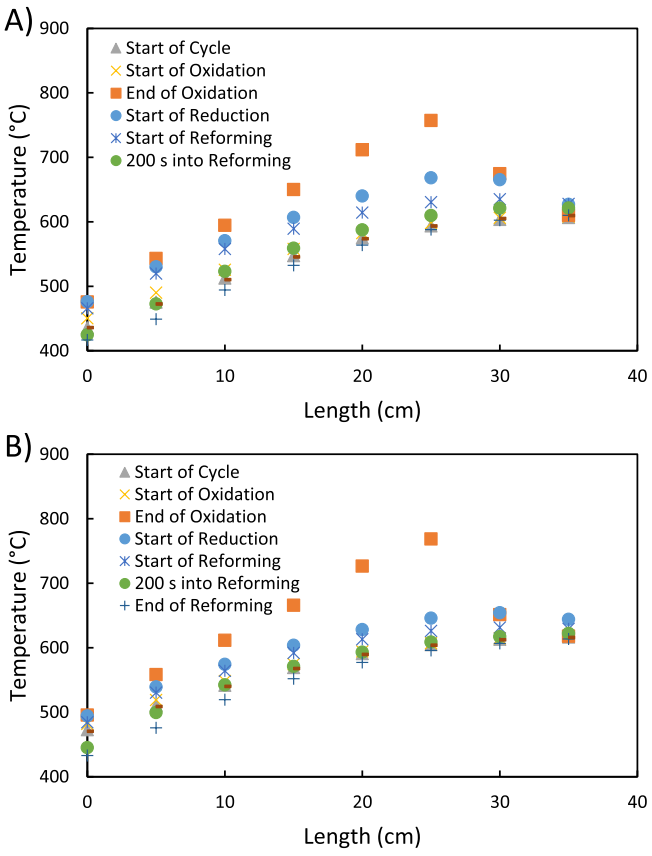

Fig. 14. Temperature profile at various times in seconds since the start of the cycle during the complete chemical looping reforming at A) 1 bar and B) 5 bar.

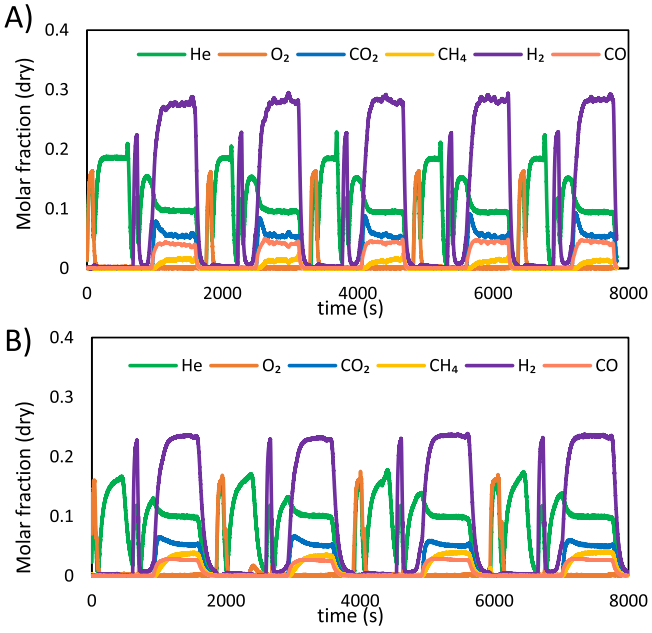

Fig. 15. A) Outlet molar fractions (dry) during 4 complete CLR cycles at 1 bar and B) 5 bar.

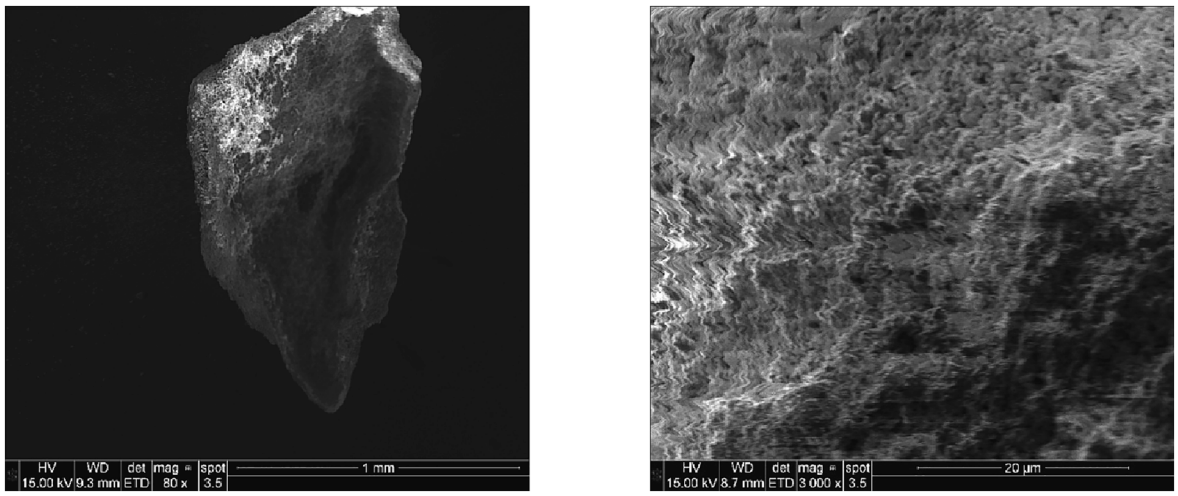

Fig. 16. SEM image of 1–1.4 mm Ni-based OC supported on calcium aluminate manufactured at 80 times magnification and 3000 times magnification.

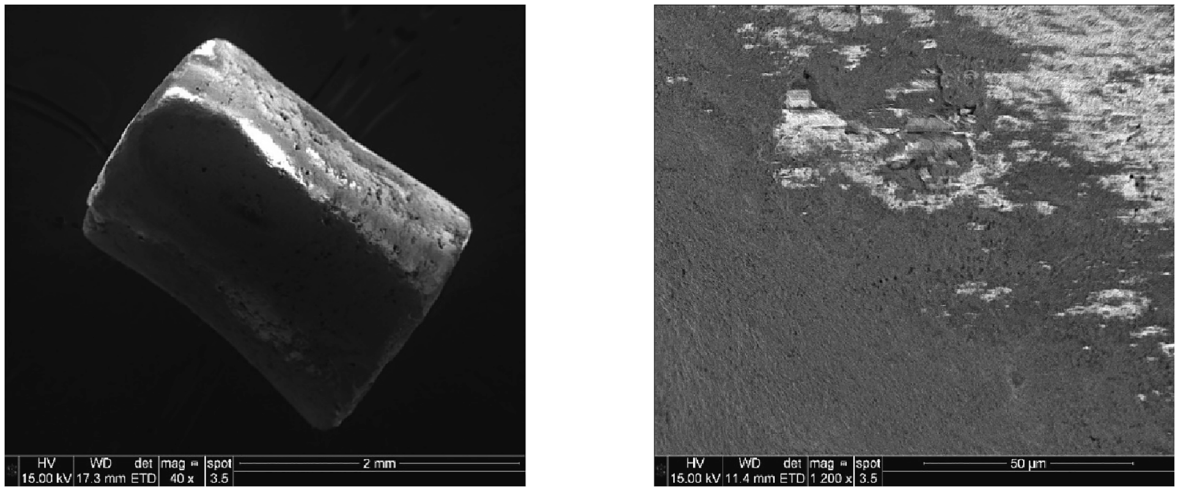

Fig. 17. SEM images of Ni-based OC on Al_2O_3 3 mm pellets, manufactured by Johnson Matthey at 40 times magnification and 1200 times magnification.

potentially showing the beginning of degradation. However, the surface of the material is much smoother without the roughness seen in Fig. 17.

4. Discussion

Chemical looping reforming of CH_4 is an effective method for the production of H_2 or syngas and the oxidation stage is capable of providing enough heat to drive the reduction and reforming stages. However, if the process is to be industrially relevant the heat management is of vital importance with the flowrates of all three stages needing close attention. This due to the large heat requirement for the reforming and necessitates adequate insulation around the reactor to minimise heat losses throughout operation.

In comparison the small amount of heat required to carry out the $C_3H_8O_3$ reforming means that higher comparative flowrates of reformate are achievable if the same heat losses occur. However, the higher temperature required to keep the $C_3H_8O_3/H_2O$ mixture as a vapour compared to the steam alone in CH_4 reforming becomes the major hurdle in industrialisation.

Both schemes also produce sufficient syngas for a fraction of the product to be used to achieve the reduction stage meaning that a hypothetical plant would require inputs of air, water and either CH_4 or $C_3H_8O_3$ and could produce separate product gasses of N_2 CO_2 waste water and syngas. This means that as long as the CO_2 was sequestered the only greenhouse gas emissions of the plant would be mainly from utilities allowing for low-carbon generation[2]. If CH_4 and $C_3H_8O_3$ are derived from biomass and used as feedstock this would constitute operational negative carbon emissions[3] once the CO2 is sent for long term storage and the indirect emissions are very limited as in the case of chemical looping reforming [29,37].

For both reforming schemes the OC's remained viable throughout, with no noticeable degradation or loss in performance. Further studies at larger scales combined with simulations should allow for upscaling to pilot and industrial scales if these hurdles can be overcome.

5. Conclusions

Reforming of $C_3H_8O_3$ and CH_4 has been demonstrated to be an effective method for syngas production. $C_3H_8O_3$ reforming was successfully tested in a reactor with a Ni-based OC that was later tested for chemical looping redox reactions. $C_3H_8O_3$ achieved full conversion with the outlet gas composition being close to the equilibrium at the temperature at the outlet of the reactor for furnace set points between 700 and 900 °C at 1 bar. The OC presented high stability after a sequence of multiple redox and reforming reactions, demonstrating that the 1st generation of oxygen carrier is already suitable for scale-up and demonstration of the technology at higher TRL levels. Moreover, both OCs did not present degradation due to thermal or chemical stress and

no carbon deposition was measured.

Similar results were shown for CH_4 reforming in a chemical looping reactor. The outlet gas composition was constrained by the thermodynamics of the reforming and water gas shift reactions. Compared to $C_3H_8O_3$ reforming, the solid temperature drop was more prominent due to the high endothermic reactions. The pseudo-continuous chemical looping CH_4 steam reforming operation has been successfully demonstrated at atmospheric and 5 bar conditions showing good repeatability in the results for several cycles and a CH_4 conversion close to the thermodynamic limit. The successful demonstration of the process in a lab-scale reactor closer to industrial reforming pressures provides a strong justification for the applicability of the process. The good conversion of CH_4 and $C_3H_8O_3$ along with the same process configuration features high flexibility of the process and in terms of feedstock co-feeding. Moreover, this process could be considered for the valorisation of waste streams from the bio-chemical industry and biogas/biomethane conversion into syngas and high-value chemicals improving the economics of those processes.

Declaration of Competing Interest

The authors declare that they have no known competing financial interests or personal relationships that could have appeared to influence the work reported in this paper.

Data availability

Data will be made available on request.

Acknowledgements

The work has received funding from the European Union's Horizon 2020 research and innovation program under grant agreement no. 884197 (GLAMOUR project). The work reflects only the authors' views and the EU is not liable for any use that may be made of the information contained therein. The authors acknowledge the Department of BEIS in the framework of the Low Carbon Hydrogen Supply 2: Stream 1 Phase 1 Competition (TRN 5044/04/2021) (RECYCLE, HYS2137) for providing funding and support to the development of this study.

Appendix A. Supplementary data

Supplementary data to this article can be found online at https://doi.org/10.1016/j.fuel.2023.129001.

References

[1] Muradov NZ, Veziroğlu TN. From hydrocarbon to hydrogen-carbon to hydrogen economy. Int J Hydrogen Energy 2005;30:225–37. https://doi.org/10.1016/j.ijhydene.2004.03.033.
[2] Shahbaz M, AlNouss A, Ghiat I, Mckay G, Mackey H, Elkhalifa S, et al. A comprehensive review of biomass based thermochemical conversion technologies integrated with CO2 capture and utilisation within BECCS networks. Resour Conserv Recycl 2021;173:105734.
[3] Stavrakas V, Spyridaki NA, Flamos A. Striving towards the Deployment of Bio-Energy with Carbon Capture and Storage (BECCS): A Review of Research Priorities and Assessment Needs. Sustain 2018, Vol 10, Page 2206 2018;10:2206. doi: 10.3390/SU10072206.
[4] Scarlat N, Dallemand JF, Fahl F. Biogas: Developments and perspectives in Europe. Renew Energy 2018;129:457–72. https://doi.org/10.1016/J.RENENE.2018.03.006.
[5] Saxena RC, Seal D, Kumar S, Goyal HB. Thermo-chemical routes for hydrogen rich gas from biomass: A review. Renew Sustain Energy Rev 2008;12:1909–27. https://doi.org/10.1016/J.RSER.2007.03.005.
[6] Attarbachi T, Kingsley M, Vincenzo Spallina. New trends on crude glycerol purification: a review. Fuel 15 May 2023;Vol 340, Page 127485 doi: 10.1016/j.fuel.2023.127485.
[7] Monteiro MR, Luis Kugelmeier C, Sanaiotte Pinheiro R, Otávio Batalha M, Da A, César S, et al. Glycerol from biodiesel production: Technological paths for sustainability. Renew Sustain Energy Rev 2018;88:109–22. https://doi.org/10.1016/J.RSER.2018.02.019.
[8] Polychronopoulou K, Charisiou N, Papageridis K, Sebastian V, Hinder S, Dabbawala A, et al. The Effect of Ni Addition onto a Cu-Based Ternary Support on the H2 Production over Glycerol Steam Reforming Reaction. Nanomater 2018, Vol 8, Page 931 2018;8:931. doi: 10.3390/NANO8110931.
[9] Charisiou ND, Papageridis KN, Siakavelas G, Sebastian V, Hinder SJ, Baker MA, et al. The influence of SiO2 doping on the Ni/ZrO2 supported catalyst for hydrogen production through the glycerol steam reforming reaction. Catal Today 2019;319:206–19.
[10] Harun N, Abidin SZ, Osazuwa OU, Taufiq-Yap YH, Azizan MT. Hydrogen production from glycerol dry reforming over Ag-promoted Ni/Al2O3. Int J Hydrogen Energy 2019;44:213–25. https://doi.org/10.1016/J.IJHYDENE.2018.03.093.
[11] Wang X, Li S, Wang H, Liu Bo, Ma X. Thermodynamic analysis of glycerin steam reforming. Energy Fuel 2008;22(6):4285–91.
[12] Liu SK, Lin YC. Generation of syngas through autothermal partial oxidation of glycerol over LaMnO3- and LaNiO3-coated monoliths. Catal Today 2014;237:62–70. https://doi.org/10.1016/j.cattod.2013.12.028.
[13] Morales-Marín A, Ayastuy JL, Iriarte-Velasco U, Gutiérrez-Ortiz MA. Nickel aluminate spinel-derived catalysts for the aqueous phase reforming of glycerol: Effect of reduction temperature. Appl Catal B Environ 2019;244:931–45. https://doi.org/10.1016/j.apcatb.2018.12.020.
[14] Bastan F, Kazemeini M, Larimi A, Maleki H. Production of renewable hydrogen through aqueous-phase reforming of glycerol over Ni/Al2O3–MgO nano-catalyst. Int J Hydrogen Energy 2018;43:614–21. https://doi.org/10.1016/j.ijhydene.2017.11.122.
[15] Shahirah MNN, Ayodele BV, Gimbun J, Cheng CK. Samarium Promoted Ni/Al2O3 Catalysts for Syngas Production from Glycerol Pyrolysis. Bull Chem React Eng Catal 2016;11:238–44. https://doi.org/10.9767/BCREC.11.2.555.238-244.
[16] Sarma SJ, Brar SK, Sydney EB, Le Bihan Y, Buelna G, Soccol CR. Microbial hydrogen production by bioconversion of crude glycerol: A review. Int J Hydrogen Energy 2012;37:6473–90. https://doi.org/10.1016/j.ijhydene.2012.01.050.
[17] P. Haussinger, R. Lohmuller AMW. 2. Production Wiley (Ed.), Ullman's Encyclopedia of Industrial Chemistry (2012), pp. 249-298,. Hydrogen, 2012.
[18] Collodi G, Azzaro G, Ferrari N, Santos S. Techno-economic Evaluation of Deploying CCS in SMR Based Merchant H2 Production with NG as Feedstock and Fuel. Energy Procedia 2017;114:2690–712.
[19] Bobadilla LF, Álvarez A, Domínguez MI, Romero-Sarria F, Centeno MA, Montes M, et al. Influence of the shape of Ni catalysts in the glycerol steam reforming. Appl Catal B Environ 2012;123-124:379–90.
[20] Schwengber CA, Alves HJ, Schaffner RA, da Silva FA, Sequinel R, Bach VR, et al. Overview of glycerol reforming for hydrogen production. Renew Sustain Energy Rev 2016;58:259–66.
[21] Abanades JC, Arias B, Lyngfelt A, Mattisson T, Wiley DE, Li H, et al. Emerging CO2 capture systems. Int J Greenh Gas Control 2015;40:126–66.
[22] Adanez J, Abad A, Garcia-Labiano F, Gayan P, De Diego LF. Progress in chemical-looping combustion and reforming technologies. Prog Energy Combust Sci 2012;38:215–82. https://doi.org/10.1016/j.pecs.2011.09.001.
[23] Luo M, Yi Y, Wang S, Wang Z, Du M, Pan J, et al. Review of hydrogen production using chemical-looping technology. Review of hydrogen production using chemical-looping technology 2018;81:3186–214.
[24] Li D, Xu R, Li X, Li Z, Zhu X, Li K. Chemical looping conversion of gaseous and liquid fuels for chemicals production: A Review. Energy Fuel 2020. https://doi.org/10.1021/acs.energyfuels.0c01006.
[25] Metcalfe IS, Ray B, Dejoie C, Hu W, de Leeuwe C, Dueso C, et al. Overcoming chemical equilibrium limitations using a thermodynamically reversible chemical reactor. Nat Chem 2019;11(7):638–43.
[26] de Leeuwe C, Hu W, Evans J, von Stosch M, Metcalfe IS. Production of high purity H2 through chemical-looping water–gas shift at reforming temperatures – The importance of non-stoichiometric oxygen carriers. Chem Eng J 2021;423:130174. https://doi.org/10.1016/J.CEJ.2021.130174.
[27] Argyris PA, Wright A, Taheri Qazvini O, Spallina V. Dynamic behaviour of integrated chemical looping process with pressure swing adsorption in small scale on-site H2 and pure CO2 production. Chem Eng J 2022;428:132606. https://doi.org/10.1016/J.CEJ.2021.132606.
[28] Stenberg V, Spallina V, Mattisson T, Rydén M. Techno-economic analysis of processes with integration of fluidized bed heat exchangers for H2 production – Part 2: Chemical-looping combustion. Int J Hydrogen Energy 2021;46:25355–75. https://doi.org/10.1016/J.IJHYDENE.2021.04.170.
[29] Lee Pereira RJ, Argyris PA, Spallina V. A comparative study on clean ammonia production using chemical looping based technology. Appl Energy 2020;280:115874. https://doi.org/10.1016/J.APENERGY.2020.115874.
[30] Gasior SJ, Forney AJ, Field JH, Bienstock D, Benson HE. Production of synthesis gas and hydrogen by the steam-iron process: pilot-plant study of fluidized and free-falling beds. Bureau of Mines 1961.
[31] Schouten JC. Chemical Reaction Engineering: History, recent developments, future scope 2009:3–4.
[32] Dudukovic MP. Frontiers in Reactor Engineering. Frontiers in reactor engineering Sci 2009;325(5941):698–701.
[33] Spallina V, Motamedi G, Gallucci F, van Sint AM. Techno-economic assessment of an integrated high pressure chemical-looping process with packed-bed reactors in large scale hydrogen and methanol production. Int J Greenh Gas Control 2019;88:71–84. https://doi.org/10.1016/j.ijggc.2019.05.026.
[34] Spallina V, Marinello B, Gallucci F, Romano MC, Van Sint AM. Chemical looping reforming in packed-bed reactors: Modelling, experimental validation and large-scale reactor design. Fuel Process Technol 2017;156:156–70. https://doi.org/10.1016/j.fuproc.2016.10.014.

[35] Argyris PA, de Leeuwe C, Abbas SZ, Amiero A, Poultson S, Wails D, et al. Chemical Looping Reforming for syngas generation at real process conditions in packed bed reactors: an experimental demonstration. Chem Eng J 2022.
[36] de Leeuwe C, Abbas SZ, Argyris PA, Zaidi A, Amiero A, Poultson S, et al. Thermochemical syngas generation via solid looping process: An experimental demonstration using Fe-based material. Chem Eng J 2023;453:139791.
[37] Argyris PA, Wong J, Wright A, Pereira LMC, Spallina V. Reducing the cost of low carbon hydrogen production via emerging chemical looping process. Energy Convers Manag 2023;277:116581.
[38] Argyris PA, de Leeuwe C, Abbas SZ, Spallina V. Mono-dimensional and two-dimensional models for chemical looping reforming with packed bed reactors and validation under real process conditions. Sustain Energy Fuels 2022;6(11):2755–70.
[39] Vaidya PD, Rodrigues AE. Glycerol reforming for hydrogen production: A review. Chem Eng Technol 2009;32(10):1463–9.
[40] Jiang Bo, Li L, Bian Z, Li Z, Othman M, Sun Z, et al. Hydrogen generation from chemical looping reforming of glycerol by Ce-doped nickel phyllosilicate nanotube oxygen carriers. Fuel 2018;222:185–92.
[41] Jiang Bo, Li L, Bian Z, Li Z, Sun Y, Sun Z, et al. Chemical looping glycerol reforming for hydrogen production by Ni@ZrO2 nanocomposite oxygen carriers. Int J Hydrogen Energy 2018;43(29):13200–11.
[42] Jiang Bo, Dou B, Song Y, Zhang C, Du B, Chen H, et al. Hydrogen production from chemical looping steam reforming of glycerol by Ni-based oxygen carrier in a fixed-bed reactor. Chem Eng J 2015;280:459–67.
[43] Dou B, Zhao L, Zhang H, Wu K, Zhang H. Renewable hydrogen production from chemical looping steam reforming of biodiesel byproduct glycerol by mesoporous oxygen carriers. Chem Eng J 2021;416:127612. https://doi.org/10.1016/J.CEJ.2020.127612.
[44] Adánez-Rubio I, Ruiz JAC, García-Labiano F, de Diego LF, Adánez J. Use of bio-glycerol for the production of synthesis gas by chemical looping reforming. Fuel 2021;288:119578. https://doi.org/10.1016/J.FUEL.2020.119578.
[45] Tippawan P, Thammasit T, Assabumrungrat S, Arpornwichanop A. Using glycerol for hydrogen production via sorption-enhanced chemical looping reforming: Thermodynamic analysis. Energy Convers Manag 2016;124:325–32. https://doi.org/10.1016/J.ENCONMAN.2016.07.018.
[46] Khazayialiabad A, Iranshahi D. Inherent CO2 capture and H2 production enhancement in a new glycerol steam reformer coupled with chemical looping combustion. Energy Fuel 2021;35:5049–63. https://doi.org/10.1021/ACS.ENERGYFUELS.0C02664/ASSET/IMAGES/LARGE/EF0C02664_0012.JPEG.
[47] Cormos AM, Dumbrava I, Cormos CC. Evaluation of techno-economic performance for decarbonized hydrogen and power generation based on glycerol thermo-chemical looping cycles. Appl Therm Eng 2020;179:115728. https://doi.org/10.1016/J.APPLTHERMALENG.2020.115728.
[48] Medrano JA, Hamers HP, Williams G, van Sint AM, Gallucci F. NiO/CaAl2O4 as active oxygen carrier for low temperature chemical looping applications. Appl Energy 2015;158:86–96. https://doi.org/10.1016/J.APENERGY.2015.08.078.
[49] Vassilis IJ. Ion exchange and adsorption fixed bed operations for wastewater treatment Part II: Scale-up and approximate design methods. J Eng Stud Res 2010;16:42–50.